Voigt circuit representation model for electrochemical impedances under finite-length diffusion conditions

C. Montella

Version of Record: https://www.sciencedirect.com/science/article/pii/S1572665720310146
Manuscript_eba82d43763fbeb0616701c48bf40674

Voigt circuit representation model for electrochemical impedances under finite-length diffusion conditions

C. Montella*

University Grenoble Alpes, University Savoie Mont Blanc, CNRS, Grenoble INP, LEPMI, 38000 Grenoble, France.

Abstract

The Voigt circuit, which is the serial association of a number of RC parallel elements, should provide an adequate description of the finite-length diffusion impedance Z_d, as conjectured and numerically experimented in previous electrochemical works. In this article, it is proved that the Voigt circuit, with infinitely many RC elements, is an exact representation model for Z_d. Next, a generalization is proposed to establish the appropriate Voigt circuit for the electrode impedance, taking into account the electron transfer reaction kinetics and the double-layer charging process at the electrode/electrolyte interface. Theoretical derivation of the Voigt circuit parameters in terms of the kinetic and mass transport parameters of the electrochemical system makes it possible to discuss the dependence of the largest time constant of the circuit on the rate constant of the electrochemical reaction, the diffusion parameters of redox species, the double-layer capacitance at the interface, and the steady-state potential imposed for EIS calculation or measurement. The theoretical predictions in this article are used in an attempt to analyze some experimental results from the electrochemical literature.

Keywords: Modeling; Impedance; EIS; Finite-length diffusion; Finite-length Warburg; Voigt circuit.

* Tel.: + 33-4-76826582; fax: + 33-4-76826630;
e-mail: Claude.Montella@lepmi.grenoble-inp.fr;
Address: Laboratoire d'Électrochimie et de Physico-chimie des Matériaux et des Interfaces (UMR 5279), Bâtiment Recherche Phelma Campus, 1130 rue de la Piscine, Domaine Universitaire BP 75, 38402 Saint Martin d'Hères, Cedex, France.

1. Introduction

The Voigt circuit, also called Foster 1 realization of RC circuits in circuit synthesis theory [1], results from n serially connected RC elements, i.e. n $\left(R_k/C_k\right)$ elements where R_k and C_k denote the k-th resistance and capacitance, respectively, and the symbol '/' means parallel association. The Voigt circuit is often employed as a representation model for Electrochemical Impedance Spectroscopy (EIS) data [2]. A series resistance R_0 is generally added to the circuit[1] to take into account the Ohmic resistances (electrolyte and connection), thus leading to the impedance:

$$Z_{\mathrm{V}}(\omega) = R_0 + \sum_{k=1}^{n} \frac{R_k}{1+\mathrm{i}\omega\tau_k} \tag{1}$$

where $\mathrm{i} = (-1)^{1/2}$, $\omega = 2\pi f$ is the angular frequency, f is the frequency, and $\tau_k = R_k C_k$ is the k-th time constant of the Voigt circuit. The condition ($\tau_1 > \tau_2 > \cdots > \tau_{n-1} > \tau_n$) is assumed in the above equation to order its successive terms.

In their pioneering work focusing on the so-called *measurement model*, Agarwal et al. [3] postulated that the Voigt circuit is a good representation model for a wide variety of electrochemical impedance spectra. As an example, starting from synthetic impedance data generated from the equivalent circuit proposed for the hydrogen evolution reaction on $\mathrm{LaNi_5}$, which includes a Finite Length Warburg (FLW) impedance, these authors demonstrated numerically that such impedance data are well fitted by the impedance in Eq. (1). They concluded that, by fitting experimental EIS data to the Voigt circuit impedance at an increasing number (n) of RC elements, the fit residuals should give access to the measurement noise of the EIS data. This was the starting point for using the Voigt circuit as the relevant measurement model to study the error structure of experimental impedance data [3-5]. Orazem and Tribollet [2] developed this approach by taking the example of EIS measurements for the ferro-ferricyanide redox couple/Pt system.

---

[1] The condition ($R_0 = 0$) used below in this article does not affect the theoretical derivations in the following Sections.

Agarwal et al. [3] also noted that the Voigt circuit impedance satisfies the Kramers-Kronig transformation. They concluded that, if experimental EIS data are well fitted by the Voigt circuit impedance, these data should also satisfy the Kramers-Kronig relationships, which is an alternative test for validation of EIS measurements.

Boukamp [6] proposed a linear fit procedure in the parameters R_k, so-called *linear KK test*, assuming that the time constants τ_k of the Voigt circuit are distributed logarithmically according to the inverse of the angular frequencies of the input signal. Hence, this author showed that a Voigt circuit including *n* RC elements could exactly represent any linear circuit at *n* experimental impedance points although no discussion of the values of the circuit parameters was provided. As pointed out by a referee of this article, "Boukamp wrote a KK test program that carries out exact approximation in all the frequency points of the data file (to check KK transforms). The program KKtest.exe might be found on the Boukamp Web page and it is also included in the free Extra Material to the EIS book [7]. The above program deals with both diffusion and kinetic-diffusion impedances".

More recently, Schönleber and Ivers-Tiffée [8] questioned about the approximability of impedance spectra by serially connected RC elements, and its implications for impedance analysis. They demonstrated that "the impedance of every possible non-oscillating electrochemical process can be approximated by a simple serial connection of generalized RC elements". They also acknowledged that RQ-, Gerischer- or Warburg-type elements could also be approximated by generalized RC elements, because of the possibility of obtaining approximated integer order models for fractional order systems [9].

The experimental approach by Lagonotte et al. [10] is quite different. Using a rotating disk electrode (RDE) device, these authors evaluated the low-frequency (LF) time constant of the ferri-ferrocyanide redox couple/Pt-RDE system using the Voigt circuit and factorized modeling to fit

their EIS measurements, with application to impedance extrapolation to zero frequency and determination of the LF capacitance of the electrochemical system. For this purpose, they focused on the best-fit estimates of Voigt circuit parameters, and, more especially, on the best-fit estimate of the first (largest) time constant $\hat{\tau}_1$ of this circuit. They observed that, by increasing the number of RC elements to $n = 6$, $\hat{\tau}_1$ seemingly converges to a constant value, unlike the other time constant estimates for $k = 2, 3, ...$ They also noted that $\hat{\tau}_1$ is nearly constant under different steady-state polarization conditions, i.e. under equilibrium as well as non-equilibrium conditions, although the associated resistance and capacitance are potential-dependent components of the Voigt circuit.

Some questions then arise. Why does the estimate of the first time constant of the best-fit Voigt circuit converge to a constant value when the number of RC elements increases to at least $n = 6$, unlike the other time constant estimates? How do the components R_1, C_1 and the time constant τ_1 connect to the mass transport process near the electrode? In other words, is it possible to predict theoretically the numerical values of R_1, C_1 and τ_1 from the electrochemical system parameters? An additional question focuses on the invariance (or not) of the time constant τ_1 upon the steady-state value of potential imposed to the electrode prior to EIS measurements.

In order to provide some answers to the above questions, we need a model for the diffusion-convection impedance of RDE. Although the FLW model is a crude approximation of the mass transport process near RDE, it provides the simplest way to explain, at least qualitatively, the experimental observations by Lagonotte et al. [10]. This point deserves to be mathematically clarified, first in the simple case where the electrode impedance is equal to the FLW impedance, and next in the more general case where the FLW impedance is an electrochemical component of equivalent circuits involving other components like the electron transfer resistance and the double-layer capacitance. It is the aim of the present work, taking the example of a one-step electrochemical reaction.

2. Finite-length Warburg impedance

The electrochemical reaction dealt with in this work is the E reaction [11] involving two soluble species, O and R, in the presence of a large excess of supporting electrolyte:

$$\mathrm{O} + z\,\mathrm{e} \leftrightarrow \mathrm{R} \tag{2}$$

The E reaction takes place on the surface of a uniformly accessible electrode, so that edge effects can be disregarded and one-dimensional diffusion conditions are satisfied in the electrolytic solution. The FLW impedance $Z_\mathrm{d}(\omega)$ results from the assumption of a constant concentration of redox species at the distance δ from the electrode surface, under static as well as dynamic conditions. This impedance is the sum of the two contributions from species O and R:

$$Z_\mathrm{d}(\omega) = Z_\mathrm{dO}(\omega) + Z_\mathrm{dR}(\omega) \tag{3}$$

For the sake of simplicity, we assume below that the diffusion coefficient is the same for both redox species, $D_\mathrm{O} = D_\mathrm{R} = D$, so that the impedances Z_dO, Z_dR and therefore Z_d have the same diffusion time constant, $\tau_\mathrm{dO} = \tau_\mathrm{dR} = \tau_\mathrm{d} = \delta^2/D$, where δ is the diffusion layer thickness.

The FLW impedance has the well-known formulation [12-14]:

$$Z_\mathrm{d}(\omega) = R_\mathrm{d} \frac{\tanh\left[(\mathrm{i}\omega\tau_\mathrm{d})^{1/2}\right]}{(\mathrm{i}\omega\tau_\mathrm{d})^{1/2}} \tag{4}$$

and the associated diffusion resistance R_d is defined as the low-frequency real limit:

$$R_\mathrm{d} = \lim_{\omega \to 0} Z_\mathrm{d}(\omega) \tag{5}$$

We will first show in Section 3 that the Voigt circuit impedance with infinitely many terms, Eq. (1) with $R_0 = 0$ and $n = \infty$, is an exact representation model for the FLW impedance, Eq. (4), in the ideal case of Nernstian redox systems investigated without double-layer charging complication. Next, we will investigate in Section 4 the effect of the double-layer charging process on the

Voigt circuit parameters. Finally, we will focus in Section 5 on the more general case of slow electron-transfer reaction kinetics for non-Nernstian redox systems.

3. Nernstian redox systems investigated without double-layer charging effect

Further simplification for EIS investigation of the E reaction results from the assumption of very fast electron transfer kinetics at the electrode surface, so-called $\mathrm{E_r}$ reaction [11] involving a Nernstian redox system. The Faradaic impedance for the $\mathrm{E_r}$ reaction is equal to the diffusion impedance, in the presence of a large excess of supporting electrolyte. Moreover, in this Section, we disregard the Ohmic potential drop in the electrolytic solution, as well as the double-layer charging process at the electrolyte/electrode interface, so that the electrode impedance is equal to the Faradaic impedance, and, therefore, to the diffusion impedance, $Z(\omega) = Z_{\mathrm{d}}(\omega)$.

Starting from the infinite product expansions of hyperbolic sine and cosine functions [15], the following formulation applies to the function $\tanh(z)/z$, with complex argument[2] z:

$$\frac{\tanh(z)}{z} = \prod_{k=1}^{\infty} \frac{1 + z^2/(k\pi)^2}{1 + 4z^2/\left[(2k-1)\pi\right]^2} \tag{6}$$

as used in our previous work [16]. Partial-fraction expansion of the above function follows directly from logarithmic differentiation of the infinite product expansion of hyperbolic cosine:

$$\frac{\tanh(z)}{z} = 8\sum_{k=1}^{\infty} \frac{1}{(2k-1)^2\pi^2 + 4z^2} \tag{7}$$

The argument $(\mathrm{i}\omega\tau_{\mathrm{d}})^{1/2}$ can be substituted for z in the above equation to derive the equivalent formulation of the FLW impedance, Eq. (4), as:

$$Z_{\mathrm{d}}(\omega) = 8R_{\mathrm{d}}\sum_{k=1}^{\infty} \frac{1}{(2k-1)^2\pi^2 + 4\mathrm{i}\omega\tau_{\mathrm{d}}} \tag{8}$$

---

[2] The usual notation for the complex argument, $z \neq \pm(2k-1)\mathrm{i}\pi/2$, should not be confused with the stoichiometric number of electron for the E reaction in Eq. (2).

which is the same as the Voigt circuit impedance in Eq. (1) where $R_0 = 0$, n is infinite, and the parameters of the k-th RC element have the relevant expressions:

$$R_k = \frac{8}{(2k-1)^2 \pi^2} R_\mathrm{d} \tag{9}$$

and:

$$\tau_k = \frac{4}{(2k-1)^2 \pi^2} \tau_\mathrm{d} \tag{10}$$

In addition, because of $\tau_k = R_k C_k$, the Voigt circuit capacitances have the same formulation irrespective of the index k:

$$C_k = \frac{\tau_\mathrm{d}}{2R_\mathrm{d}} \tag{11}$$

It is worth noticing that the time constant formulation in Eq. (10) is formally the same as that derived recently by Boukamp [17] in his work focusing on the distribution of relaxation times for the FLW impedance, although different notation is used in the two articles. In addition, the resistances R_k and the time constants τ_k decrease rapidly as the index k rises in Eqs. (9) and (10), according to the sequence $\{1, 1/9, 1/25, 1/49, 1/81, \square\}$ for both resistance and time constant ratios, R_k/R_1 and τ_k/τ_1, at k = 1, 2, 3, 4, 5, …, so that a Voigt circuit composed of the serial association of a few RC elements should be enough to represent the FLW impedance in practice.

4. Effect of double-layer charging for Nernstian redox systems

4.1. Appropriate Voigt circuit

Disregarding the Ohmic potential drop in the electrolytic solution, the electrode impedance for the $\mathrm{E_r}$ reaction, with double-layer charging effect, reads:

$$Z(\omega) = \frac{1}{\mathrm{i}\omega C_\mathrm{dl} + 1/Z_\mathrm{d}(\omega)} \tag{12}$$

where C_{dl} is the double-layer capacitance and the diffusion impedance $Z_{\mathrm{d}}(\omega)$ is given by Eq. (4). Introducing the time constant ratio:

$$r_\tau = \frac{R_{\mathrm{d}} C_{\mathrm{dl}}}{\tau_{\mathrm{d}}} \tag{13}$$

and using the extension of the Heaviside method [18] to deal with irrational impedances, as presented in the Appendix, the electrode impedance, Eq. (12), admits the partial-fraction expansion:

$$Z(\omega) = 2R_{\mathrm{d}} \sum_{k=1}^{\infty} \frac{1}{\left(1 + r_\tau + r_\tau^2 q_k^2\right)\left(q_k^2 + \mathrm{i}\omega\tau_{\mathrm{d}}\right)} \tag{14}$$

where q_k is the *k*-th positive root of the generating equation:

$$\frac{\cot q}{q} = r_\tau \tag{15}$$

The electrode impedance in Eq. (14) is the same as the Voigt circuit impedance in Eq. (1) where $R_0 = 0$, n is infinite, and the parameters of the *k*-th RC element have the relevant expressions:

$$R_k = \frac{2R_{\mathrm{d}}}{q_k^2\left(1 + r_\tau + r_\tau^2 q_k^2\right)} \tag{16}$$

and:

$$\tau_k = \frac{\tau_{\mathrm{d}}}{q_k^2} \tag{17}$$

In addition, because of $\tau_k = R_k C_k$, the *k*-th capacitance of the Voigt circuit can be derived as:

$$C_k = \frac{\tau_{\mathrm{d}}}{2R_{\mathrm{d}}}\left(1 + r_\tau + r_\tau^2 q_k^2\right) \tag{18}$$

which depends both on the index *k* and the steady-state potential imposed to the electrode through the diffusion resistance R_{d}, and, therefore, the time constant ratio r_τ in Eq. (13).

The previous results in Section 3 are recovered setting $r_\tau = 0$ in Eqs. (14)-(18). In contrast, at large enough r_τ values, Eq. (15) predicts that its first (smallest) positive root tends towards $1/\sqrt{r_\tau}$, while the other positive roots satisfy $q_k = (k-1)\pi$ for k = 2, 3, … Using Eq. (17), the time constant ratio τ_1/τ_d approaches r_τ, and therefore τ_1 is close to $R_\mathrm{d}C_\mathrm{dl}$, while the other time constants satisfy $\tau_k = \tau_\mathrm{d}/\left[(k-1)^2\pi^2\right]$ at k >1. In the same way, a glance at Eq. (16) shows that the resistance R_1 approaches R_d, while the other resistances of Voigt circuit tend towards zero. Hence, at large enough r_τ values, the appropriate Voigt circuit reduces to its first element whose impedance is $R_\mathrm{d}/(1+\mathrm{i}\omega R_\mathrm{d}C_\mathrm{dl})$. In a more general way, it can be concluded that the number of RC elements with non-vanishing impedances should decrease in the Voigt equivalent circuit for the electrode impedance at increasing r_τ values.

4.2. Effect of the steady-state current/potential

The FLW resistance has been derived for Nernstian redox systems in our textbook [19]. Assuming that $D_\mathrm{O} = D_\mathrm{R} = D$, as indicated above, one obtains the simplified formulation:

$$R_\mathrm{d} = \frac{2(1+\cosh\xi)}{z^2 f_\mathrm{N} FAm\left(c_\mathrm{O}^* + c_\mathrm{R}^*\right)} \tag{19}$$

Here z is the stoichiometric number of electron in Eq. (2), F is Faraday's constant, $f_\mathrm{N} = F/(RT)$ is the Nernst constant, R is the ideal gas constant, T is the absolute temperature, $\xi = zf_\mathrm{N}(E - E^{\circ\prime})$ is the dimensionless potential, E is the steady-state potential imposed to the electrode, $E^{\circ\prime}$ is the formal potential of redox couple, A is the electrode surface area, c_O^* and c_R^* are the initial/bulk concentrations of species O and R, respectively, and $m = D/\delta$ is the mass transport constant for redox species under steady-state conditions.

The FLW resistance for Nernstian redox systems depends on the steady-state potential through the dimensionless potential ξ in Eq. (19). Exponential increase of R_d is predicted at large

$|\xi|$ values, i.e. when the steady-state current approaches the mass-transport-limited current plateau in the anodic or cathodic direction. All parameters of the Voigt circuit, R_k, C_k and τ_k, for k = 1, 2, ..., depend on the steady-state potential through Eqs. (13) and (15)-(19). For shortening reasons, the discussion below is limited to the first time constant of the Voigt circuit, which is its largest time constant evaluated from Eq. (17) as $\tau_1 = \tau_d / q_1^2$, where q_1 is the first (smallest) positive root of Eq. (15).

The equality of the diffusion coefficients of redox species has been tacitly assumed in this article. If the following additional condition is imposed on the initial/bulk concentrations, $c_O^* = c_R^* = c^*$, for the sake of simplification, the time constant ratio derived from Eqs. (13) and (19) can be reformulated as a function of the dimensionless current ψ as:

$$r_\tau = \frac{2C_{dl}}{z^2 f_N F A \delta c^* \left(1 - \psi^2\right)} \tag{20}$$

where $\psi = I / I_{lim}$ is the ratio of the steady-state current I to the mass-transport-controlled current limit in the anodic direction ($I_{d,a} = I_{lim}$), as well as minus the current limit in the cathodic direction ($I_{d,c} = -I_{lim}$).

For illustration purpose, let us assume that EIS measurement are carried out at 25 °C for a one-electron transfer reaction (z = 1) with very fast electron-transfer reaction kinetics. Using the double-layer capacitance per unit of electrode surface area ($C_{dl}/A = 3.5 \times 10^{-5}\ \mathrm{F\ cm^{-2}}$), the initial concentration of electroactive redox species ($c^* = 2 \times 10^{-5}\ \mathrm{mol\ cm^{-3}}$) and the diffusion layer thickness ($\delta = 1.6 \times 10^{-3}\ \mathrm{cm}$), we get $r_\tau = 5.825 \times 10^{-4} / \left(1 - \psi^2\right)$ from Eq. (20). The minimum r_τ value is observed at equilibrium ($\xi = 0$ and $\psi = 0$). At the opposite, r_τ becomes infinite when $\psi \to \pm 1$, in the direction of oxidation (plus sign) or reduction (minus sign). The time constant ratio, τ_1 / τ_d, can be evaluated as a function of ψ solving numerically Eqs. (15), (17) and (20). The diffusion time constant, $\tau_d = \delta^2 / D$, only depends on the diffusion parameters D and δ, which are invariant with

the electrode potential. Hence, the graphical plot in Fig. 1 predicts that the first time constant of the Voigt circuit is nearly constant along the steady-state current-potential curve, except when the current is very close to the diffusion current plateau in the anodic or cathodic direction ($\psi \to \pm 1$). In addition, because of the very small r_τ value observed at equilibrium, i.e. $r_\tau = 5.825 \times 10^{-4}$, the nearly constant value predicted for τ_1 along the steady-state current-potential curve is close to its asymptotic value derived in Section 3 in the absence of double-layer charging effect, which is $\tau_1 = 4\tau_d / \pi^2 \approx 0.4053\ \tau_d$.

Please insert Fig. 1 at this place

5. Effect of slow electron-transfer reaction kinetics

5.1. Appropriate Voigt circuit

The E_r reaction is the hypothetical version of the E reaction pertaining to infinitely fast electron-transfer kinetics at the electrode surface. Such a condition does not hold for real systems. As a consequence, some additional complication for the Voigt circuit representation model should result from the assumption of slow electron-transfer reaction kinetics. The electrode impedance then includes the electron transfer resistance R_t, which is a potential-dependent impedance component. Disregarding the Ohmic potential drop in the electrolytic solution, the electrode impedance for the E reaction reads:

$$Z(\omega) = \frac{1}{\mathrm{i}\omega C_{dl} + 1/\left[R_t + Z_d(\omega)\right]} \tag{21}$$

where the diffusion impedance is still given by Eq. (4). We introduce the resistance ratio:

$$r_R = \frac{R_t}{R_d} \tag{22}$$

which depends on the electron transfer reaction kinetics, the mass transport conditions and the steady-state potential imposed to the electrode. Using the same simplifications as in Section 4, i.e. $D_{\mathrm{O}} = D_{\mathrm{R}} = D$ and $c_{\mathrm{O}}^{*} = c_{\mathrm{R}}^{*} = c^{*}$, the resistance ratio is maximum at the equilibrium potential of the electrode. This ratio tends towards zero as the current approaches the diffusion current plateau in the anodic or cathodic direction ($\psi \to \pm 1$). Derivation of the Voigt circuit representation model for the electrode impedance in Eq. (21) follows the same calculation procedure as in Section 4.1 and in the Appendix, although the theoretical formulations are more intricate than the previous ones.

The successive positive roots q_k of the following equation, which is the generalization of Eq. (15) to the case of non-Nernstian redox systems ($r_R \neq 0$), generate the poles $p_k = -q_k^2 / \tau_{\mathrm{d}}$:

$$\frac{\cot q}{q\left(1 + r_R q \cot q\right)} = r_\tau \tag{23}$$

while the generating equation for the impedance zeros, $z_k = -q_{\mathrm{z},k}^2 / \tau_{\mathrm{d}}$, is:

$$q_z \cot q_z = -1 / r_R \tag{24}$$

irrespective of r_τ. The electrode impedance in Eq. (21) admits the following infinite product expansion where R_{p} denotes the polarization resistance, $R_{\mathrm{p}} = R_{\mathrm{t}} + R_{\mathrm{d}}$:

$$Z(\omega) = R_{\mathrm{p}} \prod_{k=1}^{\infty} \frac{1 - \mathrm{i}\omega / z_k}{1 - \mathrm{i}\omega / p_k} \tag{25}$$

In addition, the locations of poles and zeros in Fig. 2 have the same features as those in Fig. A.1 of the Appendix. Hence, the electrode impedance in Eq. (21) and (25) can be realized as a RC network.

Please insert Fig. 2 at this place

In fine, the Voigt circuit, with $n = \infty$, is an exact representation model for the electrochemical impedance $Z(\omega)$ in Eq. (21). Its *k*-th time constant is given by Eq. (17) using the *k*-th positive root q_k of Eq. (23). The *k*-th resistance can be derived as:

$$R_k = \frac{2R_\mathrm{d}\left(1+r_R q_k \cot q_k\right)}{q_k^2\left[1+\dfrac{\cot q_k}{q_k}+\left(\cot q_k\right)^2 - r_R r_\tau q_k^2\left(1-\dfrac{\cot q_k}{q_k}+\left(\cot q_k\right)^2\right)\right]} \tag{26}$$

used together with Eq. (23). Finally, because of $\tau_k = R_k C_k$, the *k*-th capacitance of the Voigt circuit is given by:

$$C_k = \frac{\tau_\mathrm{d}}{2R_\mathrm{d}} \cdot \frac{1+\dfrac{\cot q_k}{q_k}+\left(\cot q_k\right)^2 - r_R r_\tau q_k^2\left(1-\dfrac{\cot q_k}{q_k}+\left(\cot q_k\right)^2\right)}{1+r_R q_k \cot q_k} \tag{27}$$

also used with Eq. (23). The Voigt circuit parameters formulated from Eqs. (17), (23), (26) and (27) depend on the index *k*, the mass transport parameters, the electron transfer reaction kinetics, the initial concentration of redox species, the double-layer capacitance, and the steady-state potential imposed to the electrode, which are involved in the time constant ratio r_τ, Eq. (13), and the resistance ratio r_R, Eq. (22). The simplified formulations of R_k, C_k and τ_k derived in Section 3 are recovered setting $r_R = 0$ and $r_\tau = 0$, while the intermediate formulations derived in Section 4.1 result from the condition $r_R = 0$.

The approximating (truncated) version of Eq. (25), limited to its first *n* terms, is:

$$Z_{\mathrm{ap},1}(n,\omega) = R_\mathrm{p}\prod_{k=1}^{n}\frac{1-\mathrm{i}\omega/z_k}{1-\mathrm{i}\omega/p_k} \tag{28}$$

It can be compared to the following approximation resulting from the Voigt circuit representation model:

$$Z_{\mathrm{ap},2}(n,\omega) = R_\mathrm{p} - \sum_{k=1}^{n} R_k + \sum_{k=1}^{n}\frac{R_k}{1-\mathrm{i}\omega/p_k} \tag{29}$$

The rates of convergence of the two approximations towards the electrode impedance $Z(\omega)$ are compared in Fig. 3. Clearly, the approximation based on the Voigt circuit is the most efficient because of its higher convergence rate.

Please insert Fig. 3 at this place

5.2. Effect of the steady-state current/potential

We focus again on the first (largest) time constant of the Voigt circuit, $\tau_1 = \tau_d / q_1^2$, where q_1 is the first (smallest) positive root of Eq. (23), which depends both on the time constant ratio r_τ in Eq. (13) and the resistance ratio r_R in Eq. (22). Usual impedance calculation rules [20] provide the theoretical formulations of the resistances R_t and R_d for the E reaction, and, therefore, the theoretical formulations of the dimensionless parameters r_R and r_τ. For the sake of simplicity, we assume below the same diffusion coefficient for both redox species, $D_O = D_R = D$, the same initial concentration of redox species, $c_O^* = c_R^* = c^*$, and the same symmetry factor for the electron transfer reaction in the direction of oxidation (subscript 'o') and reduction (subscript 'r'), $\alpha_o = \alpha_r = 1/2$. The resistance ratio, $r_R = R_t / R_d$, takes on the following simplified formulation where k° is the standard rate constant of the electrochemical reaction, $m = D/\delta$ is the mass transport constant of redox species under steady-state conditions, and $\xi = z f_N (E - E^{\circ\prime})$ is the dimensionless potential:

$$r_R = \frac{1}{2(k^\circ/m)\cosh(\xi/2)} \tag{30}$$

Using the same simplifications as above, the time constant ratio, $r_\tau = R_d C_{dl} / \tau_d$, can be derived as:

$$r_\tau = \frac{(1+\cosh\xi) C_{dl}}{z^2 f_N F A \delta c^*} \cdot \frac{2(k^\circ/m) + \operatorname{sech}(\xi/2)}{2(k^\circ/m) + \cosh(\xi/2)} \tag{31}$$

where sech(.) denotes the hyperbolic secant that is the reciprocal of hyperbolic cosine. The first time constant of Voigt circuit can be evaluated from Eqs. (17), (23), (30) and (31) as a function of the standard rate constant (k°) of the electrochemical reaction, the mass transport parameters (D and δ), the initial concentration (c^*) of redox species, the double-layer capacitance (C_{dl}) and the steady-state potential (E) imposed to the electrode through the dimensionless potential ξ.

Several asymptotic limits are of interest for this time constant. First, $\tau_1 = 4\,\tau_d/\pi^2$ has been predicted in Section 3 for Nernstian redox systems ($r_R = 0$) investigated without double-layer charging effect ($r_\tau = 0$). Next, $\tau_1 = R_d C_{dl}$ has been predicted in Section 4.2 at large r_τ values and negligible r_R values. A third possible expression is $\tau_1 = R_t C_{dl}$ when the resistance ratio r_R is very large. Another limiting expression is $\tau_1 = \left(R_t + R_d\right) C_{dl}$. The validity domains for those formulations can be visualized by plotting the zone diagram in Fig. 4 with log-log coordinates. In each zone of Fig. 4, the relative deviation of the time constant τ_1 from its asymptotic formulation is less than 5 %. It is worth noticing that the validity domain for the limiting formulation ($\tau_1 = 4\,\tau_d/\pi^2$) on bottom side of the zone diagram covers the case of ideal Nernstian systems ($r_R = 0$) investigated in Section 3, as well as the case of non-Nernstian systems ($r_R > 0$) investigated in this Section, provided that the time constant ratio, $r_\tau\left(1 + r_R\right) = \left(R_t + R_d\right) C_{dl}/\tau_d$, is low enough.

Please insert Fig. 4 at this place

Given numerical values for the dimensionless kinetic parameter, $\Lambda = k^\circ/m$, and the dimensionless capacitive parameter, $K = C_{dl}/\left(z^2 f_N F A \delta c^*\right)$, the equilibrium condition ($\xi = 0$, subscript 'eq') for τ_1 is represented in the zone diagram by the dot with coordinates $\log r_{R,eq} = -\log\left(2\Lambda\right)$ and $\log r_{\tau,eq} = \log\left(2K\right)$, on bottom side of Fig. 4. If the steady-state potential *E* is increased or decreased with respect to its equilibrium value, which corresponds to increasing $|\xi|$ values in Eqs. (30) and (31), the characteristic point, with coordinates $\log r_R$ and $\log r_\tau$, moves away from its equilibrium position in the zone diagram. The trace left by the moving point is the curve, so-called *trajectory* below, whose equation can be derived by elimination of the dimensionless potential ξ between Eqs. (30) and (31) as:

$$\log r_\tau = \log\left(2K\right) + \log\frac{1 + 1/r_R}{1 + 4\Lambda^2 r_R} \tag{32}$$

It is worth noticing that the asymptotic moving direction at very small r_R values is $\log(2K) - \log r_R$, irrespective of the Λ value.

Three examples of trajectories are plotted in the zone diagram of Fig. 4, for $K = 10^{-3}$ and $\Lambda = 10^{-3}$, 2 and 8.5, which corresponds, respectively, to very slow, intermediate and fast electron-transfer reaction kinetics. The intersections of those trajectories with the limiting zones of the zone diagram make it possible to predict the possible sequences of τ_1 formulations/values that can be observed when the steady-state potential moves away from its equilibrium value. Keeping in mind that the electron transfer resistance R_t and the diffusion resistance R_d are potential-dependent components of the electrode impedance, the first time constant of the Voigt equivalent circuit is nearly constant only when it is close to $4\tau_d/\pi^2$ in the bottom zone of Fig. 4. Another information, derived from the observation of Fig. 4, is that the asymptotic formulations/values of the first time constant, $(R_t + R_d)C_{dl}$ and $R_d C_{dl}$, although mathematically predictable, are unlikely to be observed in practice.

5.3. Attempt analysis of previous experimental results from the literature

Here we focus on the recent article by Lagonotte et al. [10], which is concerned with the Voigt circuit representation model of the electrode impedance for the ferro-ferricyanide redox couple/Pt-RDE system. As indicated in the introduction Section of this article, the above authors investigated this electrochemical system using the Voigt circuit and factorized modeling to fit their EIS data. They focused more especially on the best-fit estimate $\hat{\tau}_1$ of the first (largest) time constant of the Voigt circuit[3]. They observed that, by increasing the number of RC elements to n = 6, $\hat{\tau}_1$ seemingly converges to a constant value, unlike the other estimates of time constants for k = 2,

[3] In practice, Lagonotte et al. [10] evaluated the estimates of the poles ($\hat{p}_k$ for $k = 1, 2, ..., n$) of the Voigt circuit impedance, using an appropriate fitting procedure. The time constant estimate $\hat{\tau}_k$ is equal to minus the reciprocal of $\hat{p}_k$.

3, … They also noted that the converged value of $\hat{\tau}_1$ is nearly constant under different steady-state polarization conditions, i.e. under equilibrium as well as non-equilibrium conditions.

The finite-length diffusion model is often employed as an approximation of the diffusion-convection process near RDE, with the diffusion layer thickness δ being replaced by the characteristic length of diffusion-convection derived by Levich [21]. Thus, the theoretical predictions in this work can be applied, at least as a first approach, to the experimental observations by Lagonotte et al. [10].

Let us consider the Nyquist graph for the electrode impedance $Z(\omega)$ in Fig. 5(a), which has been plotted from Eqs. (4) and (21) using the parameter values given in the captions. The frequency range explored satisfies $\left(-2 \le \log\left(f/\mathrm{Hz}\right) \le 4\right)$ at a spacing of 9 impedance calculations per decade. The impedance graph mimics, at least roughly, the Nyquist graph plotted by Lagonotte et al. at the equilibrium potential of the Pt electrode (see Fig. 3 of Ref. [10]).

The EIS data can be fitted using the impedance model in Eq. (1). For this purpose, we use noise-free[4] unweighted[5] impedance data together with the Levenberg-Marquardt algorithm implemented in the 'NonlinearModelFit' built-in function of *Mathematica* [22]. The fit residuals are shown in Fig. 5(b).

Please insert Fig. 5 at this place

[4] "Noise-free impedance data" means that no random noise has been added before fitting the impedance. Of course, the computational noise of the synthetic impedance data is present. The impact of additional random noise on the complex nonlinear least squares fit could be evaluated numerically without major difficulty, but it is not the aim of this work. The use of noise-free EIS data makes it possible to study the convergence of the best-fit estimates of the Voigt circuit parameters to their asymptotic values at large enough numbers of Voigt elements (see Fig. 6).

[5] Proportional and modulus-based weighting strategies yield nearly the same best-fit parameter estimates as unitary weighting for the leading RC elements of the Voigt circuit.

Good visual agreement is observed between the synthetic EIS data and the Voigt circuit impedance at $n \geq 4$, in agreement with Lagonotte et al.'s observations [10]. A Voigt circuit with 6 serially connected RC elements has been used to fit the impedance data in Fig. 5. At increasing values of *n*, the best-fit estimate $\hat{\tau}_1$ converges to its asymptotic value τ_1 predicted from the set of Eqs. (17), (23), (30) and (31). The rate of convergence is illustrated in Fig. 6 by plotting the decimal logarithm of the absolute value of relative deviation of $\hat{\tau}_1$ from τ_1 as a function of *n*. Rapid convergence is observed. Similar convergence is noted for $\hat{R}_1$ to R_1 (not shown in the Figure). In contrast, the convergence rate is slower for the parameter estimates of the second RC element, as illustrated for $\hat{\tau}_2$ in the same Figure. At small values of *n*, e.g. *n* = 6 in Ref. [10], the estimate of the first time constant approaches its asymptotic value with less than 1 ‰ relative deviation, unlike the estimate of the second time constant because of its slower convergence rate. Indeed, the relative deviation of $\hat{\tau}_2$ from τ_2 is close to 5 % at *n* = 6. This qualitatively agrees with the experimental observations by Lagonotte et al. [10]. However, the experimental rate of convergence of $\hat{\tau}_1$ to τ_1 in Ref. [10] is slower than that predicted in Fig. 6 of this article. We should be aware, here, of the weakness of the FLW model to accurately describe the diffusion-convection process near RDE. This point deserves to be further analyzed in a forthcoming article [23], starting from a more efficient model of the diffusion-convection impedance for RDE.

Please insert Fig. 6 at this place

Next, we look at the dependence of $\hat{\tau}_1$ on the steady-state potential imposed for EIS computation/measurement. The left-side trajectory (blue curve) in the zone diagram of Fig. 4 has been plotted using the same parameter values as in Fig. 5. The time constant τ_1 evaluated along this trajectory is predicted to be nearly constant (with less than 5 % deviation) in the interval $|\psi| \leq 0.93$. The same condition applies to the converged value of its best-fit estimate $\hat{\tau}_1$. This should explain

the nearly constant value of $\hat{\tau}_1$ obtained by Lagonotte et al. at the three steady-state potentials imposed in Fig. 2 of Ref. [10].

6. Conclusion

First, the Voigt circuit, with infinitely many RC elements, is an exact representation model for the electrode impedance pertaining to the E reaction investigated on a uniformly accessible electrode under finite-length diffusion conditions for redox species in the electrolyte. This fully validates the conjecture in the seminal work by Agarwal et al. [3]. The generalized Heaviside method presented in the Appendix provides a general way to derive the analytical expressions of the Voigt circuit parameters (resistances, capacitances and related time constants) as a function of the kinetic rate constant of the electrochemical reaction, the mass transport parameters, the initial concentrations of redox species, the double-layer capacitance at the interface, and the steady-state potential imposed to the electrode. Application to Nernstian redox systems investigated without or with double-layer charging effect, as well as to non-Nernstian redox systems involving slow electron-transfer reaction kinetics, has been presented in this article as illustration examples.

Exact representation, at any frequency, of electrochemical impedances involving a finite-length diffusion component requires infinitely many RC elements in the Voigt equivalent circuit. Fairly accurate approximation of such impedances by the Voigt circuit is less demanding and requires only a few RC elements, as illustrated by the complex nonlinear least squares fits of synthetic EIS data performed in this work. The minimum number ($n_{\min}$) of RC elements required for approximation of the electrode impedance for the E reaction on RDE at any frequency depends on the approximation level demanded, and, in addition, on the resistance ratio, $r_R = R_t/R_d$, and the time constant ratio, $r_\tau = R_d C_{dl}/\tau_d$. As a general rule, the number $n_{\min}$ of RC elements should decrease at increasing values of r_R and/or r_τ. At the limit, the condition ($n_{\min} = 1$) should apply in the upper

zones of the zone diagram of Fig. 4 where the Nyquist graph for the electrode impedance approaches a semi-circle graph.

Next, we have been focusing on the first (largest) time constant τ_1 of the Voigt circuit, and on its dependence on the steady-state potential imposed to the electrode for EIS calculation or measurement. Nearly invariance of τ_1 with respect to the electrode potential has been predicted for Nernstian redox systems investigated without double-layer charging effect, as well as for non-Nernstian redox systems when the time constant ratio, $\left(R_t + R_d\right)C_{dl}/\tau_d$, takes on a low enough value. This applies in practice to fast or intermediate electron-transfer reaction kinetics when EIS measurements are carried out not too far from the equilibrium potential, because of the linear proportionality of τ_1 with the diffusion-convection time constant in this case, i.e. $\tau_1 = 4\,\tau_d/\pi^2$. Clearly, such conditions were satisfied in the experimental work of Lagonotte et al. [10], which explains the nearly constant value of $\hat{\tau}_1$ observed by these authors under equilibrium as well as non-equilibrium conditions. Other asymptotic formulations are possible for this time constant depending on the electrochemical system considered and the experimental conditions, as summarized in the zone diagram of Fig. 4. Looking at this diagram, all possible sequences of asymptotic formulations/values of the time constant τ_1, and therefore of the converged value of its best-fit estimate $\hat{\tau}_1$, can be predicted when the electrode potential moves away from its equilibrium value.

The theoretical derivations and conclusions presented in this article apply to finite-length diffusion of redox species in the electrolytic solution. In addition, they provide a first (rough) approach to the Voigt circuit representation model for the impedance of uniformly accessible rotating disk electrodes. More elaborate models have been proposed in the electrochemical literature [2,24-26] to accurately describe the diffusion-convection impedance for RDE. The impact of such models on the appropriate Voigt circuit representation model for the electrode impedance will be analyzed in a forthcoming article [23].

Appendix

Using the Heaviside expansion method [18], strictly proper rational functions of the Laplace variable p:

$$H(p) = \frac{f(p)}{g(p)} \tag{A.1}$$

whose only singularities are simple real poles p_k, for $k = 1, 2, ..., n$, can be expanded into partial fractions as:

$$H(p) = \sum_{k=1}^{n} \frac{\mathrm{res}(p_k)}{p - p_k} \tag{A.2}$$

where the residue of the k-th pole is given by:

$$\mathrm{res}(p_k) = \frac{f(p_k)}{g'(p_k)} \tag{A.3}$$

provided that $g'(p_k) = \mathrm{d}g(p)/\mathrm{d}p\big|_{p=p_k} \neq 0$. Let us consider the class of electrochemical models whose impedance $Z(p)$ can be substituted for $H(p)$ in Eqs. (A.1) and (A.2). We get the Voigt circuit impedance in Eq. (1), with $R_0 = 0$:

$$Z(p) = Z_{\mathrm{V}}(p) = \sum_{k=1}^{n} \frac{R_k}{1 + p\tau_k} \tag{A.4}$$

where the k-th resistance, capacitance and time constant have the following expressions:

$$R_k = -\frac{\mathrm{res}(p_k)}{p_k},\ C_k = \frac{1}{\mathrm{res}(p_k)} \text{ and } \tau_k = R_k C_k = -\frac{1}{p_k} \tag{A.5}$$

Many irrational transfer functions for spatially distributed systems admit a partial-fraction expansion like that in Eqs. (A.1)-(A.5), with infinitely many poles ($n \to \infty$) [27]. The electrochemical impedances investigated in this article belong to this class. The electrode impedance derived from Eqs. (4) and (12) takes on the form of Eq. (A.1) where $f(p) = R_{\mathrm{d}}$ and $g(p)$ is the function:

$$g(p) = pR_{\mathrm{d}}C_{\mathrm{dl}} + (p\tau_{\mathrm{d}})^{1/2} \coth\left[(p\tau_{\mathrm{d}})^{1/2}\right] \tag{A.6}$$

The impedance $Z(p)$ has an infinite number of simple real poles p_k, which are the roots of the equation:

$$g(p_k) = p_k R_{\mathrm{d}}C_{\mathrm{dl}} + (p_k\tau_{\mathrm{d}})^{1/2} \coth\left[(p_k\tau_{\mathrm{d}})^{1/2}\right] = 0 \tag{A.7}$$

Those poles should have negative values so that the condition ($\tau_k > 0$) applies to the RC elements of the Voigt circuit. Hence, we can write $(p_k\tau_{\mathrm{d}})^{1/2} = \mathrm{i}q_k$, with real q_k, and, therefore:

$$p_k = -\frac{q_k^2}{\tau_{\mathrm{d}}} \tag{A.8}$$

Using the identity $\coth(\mathrm{i}q_k) = -\mathrm{i}\cot q_k$, Eq. (A.7) provides the generating equation for q_k:

$$\frac{\cot q_k}{q_k} = r_\tau = \frac{R_{\mathrm{d}}C_{\mathrm{dl}}}{\tau_{\mathrm{d}}} \tag{A.9}$$

and the impedance poles follow from Eq. (A.8) for *k* = 1, 2, …, while the impedance zeros are equal to $-k^2\pi^2/\tau_{\mathrm{d}}$, irrespective of the r_τ value. The locations of poles and zeros in Fig. A.1(b) shows that (i) all poles and zeros are simple and lie on the negative real axis of the complex (*p*) plane, (ii) the poles and zeros are interlaced, and (iii) the first location on the negative real axis (i.e. the smallest absolute value) is that of a pole.

Please insert Fig. A.1 at this place

Calculus of residues, from Eq. (A.3), requires the derivative of the function $g(p)$. One obtains from Eq. (A.6):

$$g'(p) = R_{\mathrm{d}}C_{\mathrm{dl}} + \frac{\tau_{\mathrm{d}}}{2}\left\{\frac{\coth\left[(p\tau_{\mathrm{d}})^{1/2}\right]}{(p\tau_{\mathrm{d}})^{1/2}} - \mathrm{csch}\left[(p\tau_{\mathrm{d}})^{1/2}\right]^2\right\} \tag{A.10}$$

where $\mathrm{csch}(z) = 1/\sinh(z)$ denotes the hyperbolic cosecant. Using again $(p_k\tau_{\mathrm{d}})^{1/2} = \mathrm{i}q_k$, and $\coth(\mathrm{i}q_k) = -\mathrm{i}\cot q_k$, together with Eq. (A.9) and the identity $\mathrm{csch}(\mathrm{i}q_k) = -\mathrm{i}\csc q_k = -\mathrm{i}/\sin q_k$, the residue of the *k*-th pole can be derived from Eq. (A.3) as:

$$\mathrm{res}\left(p_k\right)=\frac{2R_\mathrm{d}/\tau_\mathrm{d}}{1+r_\tau+r_\tau^2 q_k^2} \tag{A.11}$$

From Eq. (A.11), (iv) the residues at the poles of the electrode impedance are real and positive. The properties (i)-(iv) above are those of RC network impedances [1, p. 73]. The relevant expressions for the *k*-th parameters of the Voigt circuit reported in Eqs. (16)-(18) of the article result from Eqs. (A.5), (A.8) and (A.11). Moreover, setting $r_\tau=0$ in the absence of double-layer charging effect, we get $q_k=\left(2k-1\right)\pi/2$ from Eq. (A.9), $p_k=-\left(2k-1\right)^2\pi^2/\left(4\tau_\mathrm{d}\right)$ from Eq. (A.8), and $\mathrm{res}\left(p_k\right)=2R_\mathrm{d}/\tau_\mathrm{d}$ from Eq. (A.11), so that the partial-fraction expansion of the finite-length diffusion impedance in Eq. (8) is recovered using Eqs. (A.4) and (A.5).

Declaration of competing interest

The author declares that he has no known competing financial interests or personal relationships that could have appeared to influence the work reported in this paper.

CRediT authorship contribution statement

Claude Montella: Conceptualization, Methodology, Formal analysis, Visualization, Writing original draft.

References

[1] G.C. Temes, J.W. LaPatra, Introduction to Circuit Synthesis and Design, McGraw-Hill, Inc., New York, 1977.

[2] M. E. Orazem, B. Tribollet, Electrochemical Impedance Spectroscopy, second ed., John Wiley & Sons, Inc., Hoboken, New Jersey, 2017.

[3] P. Agarwal, M.E. Orazem, L.H. Garcia-Rubio, Measurement Models for Electrochemical Impedance Spectroscopy, I. Demonstration and Applicability, J. Electrochem. Soc. 139 (1992) 1917-1927.

[4] P. Agarwal, O.D. Crisalle, M.E. Orazem, L.H. Garcia-Rubio, Application of Measurement Models to Impedance Spectroscopy: II. Determination of the Stochastic Contribution to the Error Structure, J. Electrochem. Soc. 142 (1995) 4149-4158.

[5] P. Agarwal, M.E. Orazem, L.H. Garcia-Rubio, Application of Measurement Models to Impedance Spectroscopy: III. Evaluation of Consistency with the Kramers-Kronig Relations, J. Electrochem. Soc. 142 (1995) 4159-4168.

[6] B.A. Boukamp, A linear Kronig-Kramers Transform Test for Immitance Data Validation, J. Electrochem. Soc. 142, (1995) 1885-1894.

[7] A. Lasia, Electrochemical impedance spectroscopy and its applications, Springer, 2014.

[8] M. Schönleber, E. Ivers-Tiffée, Approximability of impedance spectra by RC elements and implications for impedance analysis, Electrochem. Com. 58 (2015) 15-19.

[9] B.V. Vinagre, I. Podlubny, A. Hernández, V. Feliu, Some Approximations of Fractional Order Operators used in Control Theory and Applications, J. Fractional Calculus Appl. Anal. 4 (2000) 47-66.

[10] P. Lagonotte, V.A. Raileanu Ilie, S. Martemianov, A. Thomas, Extrapolation to zero frequency with first time constant of ferri-ferrocyanide/Pt interface using Foster equivalent circuit and factorized Modeling, J. Electroanal. Chem. 839 (2019) 256-263.

[11] A.J. Bard, L.R. Faulkner, Electrochemical Methods. Fundamentals and Applications, second ed., John Wiley & Sons, Inc., New York, 2001.

[12] J. Llopis, F. Colom, Study of the Impedance of a Platinum Electrode Acting as Anode, in Proceeding of the Eighth Meeting of the C.I.T.C.E., 1956, Butterworths, London, 1958, p. 414-427.

[13] P. Drossbach, J. Schultz, Elektrochemische untersuchungen an kohleelektroden—I: Die überspannung des wasserstoffs, Electrochim. Acta 11 (1964) 1391-1404.

[14] D. Schuhmann, Sur l'impédance de diffusion en basse fréquence, Compt. Rend. Acad. Sci. (Paris) 262 Série C (1966) 624-627.

[15] https://dlmf.nist.gov/4.36#E2, Accessed 1 February 2020.

[16] F. Berthier, J.-P. Diard, C. Montella, Hopf bifurcation and sign of the transfer resistance, Electrochim. Acta 44 (1999) 2397-2404.

[17] B.A. Boukamp, Derivation of a Distribution of Relaxation Times for the (fractal) Finite Length Warburg, Electrochim. Acta 252 (2017) 154-163.

[18] A. Angot, Compléments de Mathématiques, 6^{ième} ed., Masson et C^{ie}, Paris, 1972.

[19] C. Montella, J.-P. Diard, B. Le Gorrec, Exercices de cinétique électrochimique, II. Méthode d'impédance, Hermann, Paris, 2005, p. 211.

[20] J.-P. Diard, B. Le Gorrec, C. Montella, Cinétique électrochimique, Hermann, Paris, 1996.

[21] V.G. Levich, Physicochemical Hydrodynamics, Prentice-Hall, Inc., Englewood Cliffs, N. J., 1962.

[22] https://www.wolfram.com/mathematica/, Accessed 1 February 2020.

[23] C. Montella, submitted for publication, J. Electroanal. Chem.

[24] B. Tribollet, J. Newman, The modulated Flow at a Rotating Disk Electrode, J. Electrochem. Soc. 130 (1983) 2016-2026.

[25] R. Michel, C. Montella, Diffusion–convection impedance using an efficient analytical approximation of the mass transfer function for a rotating disk, J. Electroanal. Chem. 736 (2015) 139-146.

[26] J.-P. Diard, C. Montella, Re-examination of the diffusion–convection impedance for a uniformly accessible rotating disk. Computation and accuracy, J. Electroanal. Chem. 742 (2015) 37-46.

[27] R. Curtain, K. Morris, Transfer Functions of Distributed Parameter Systems: A Tutorial, Automatica 45 (2009) 1101-1116.

Figures

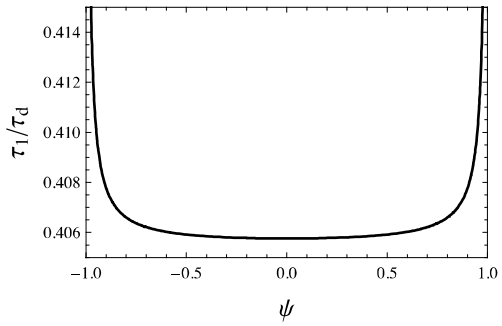

Fig. 1: Dependence of the time constant ratio (τ_1/τ_d) on the normalized steady-state current ($\psi = I/I_{lim}$). The time constant ratio is calculated from Eqs. (15), (17) and (20), using the parameter values given in the text.

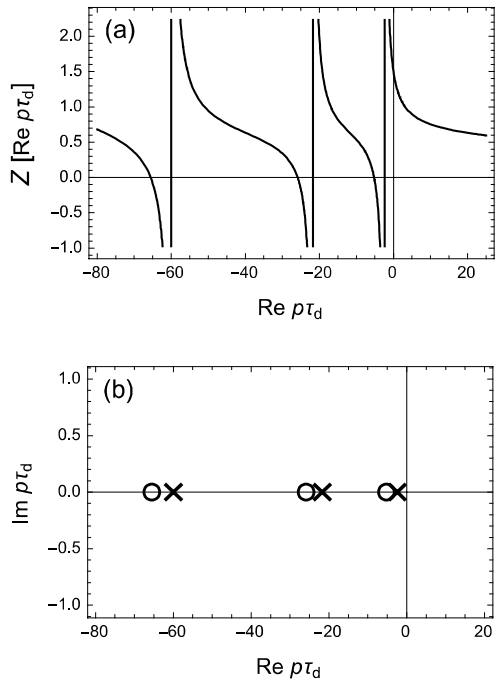

Fig. 2: (a) Real-*p* impedance and (b) the first three poles (crosses) and three zeros (circles) of the dimensionless impedance, $Z(p)/R_d = \left\{ p\tau_d r_\tau + 1 \Big/ \left[r_R + (p\tau_d)^{-1/2} \tanh\left[(p\tau_d)^{1/2} \right] \right] \right\}^{-1}$, calculated from Eqs. (4) and (21) at $r_R = 0.5$ and $r_\tau = 0.01$.

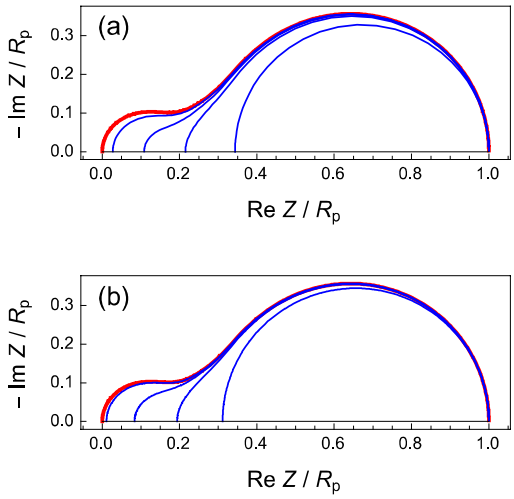

Fig. 3: Convergence test for the two truncated formulations of the electrode impedance either based on (a) product expansion of the impedance in Eq. (28), or (b) partial fraction expansion of the impedance in Eq. (29). Parameter values: $r_{\mathrm{R}} = 0.2$ and $r_{\tau} = 0.01$. Nyquist graph of the normalized electrode impedance (red curve). Nyquist graphs of the normalized impedance approximations (blue curves) with (a) n = 1, 3, 9, 18 from right to left, and (b) n = 1, 3, 7, 9 from right to left. For interpretation of the references to colors in the figure captions, the reader is referred to the Web version of this article.

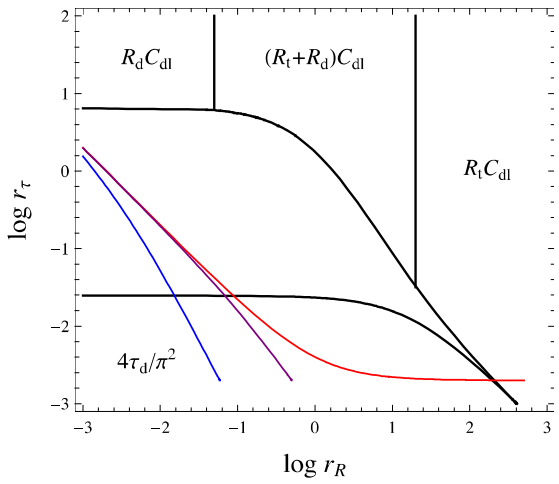

Fig. 4: Zone diagram for the first (largest) time constant τ_1 of the Voigt circuit representing the electrode impedance in Eq. (21). Three trajectories are plotted for $K = 10^{-3}$ and $\Lambda = 10^{-3}$ (red curve), 2 (purple curve) and 8.5 (blue curve) at increasing $|\xi|$ and $|\psi|$ values from right to left. The associated colored dots correspond to the normalized steady-state current values, $|\psi| = 0$, 0.5, 0.9 and 0.99, from right to left and bottom to top. For interpretation of the references to colors in the figure captions, the reader is referred to the Web version of this article.

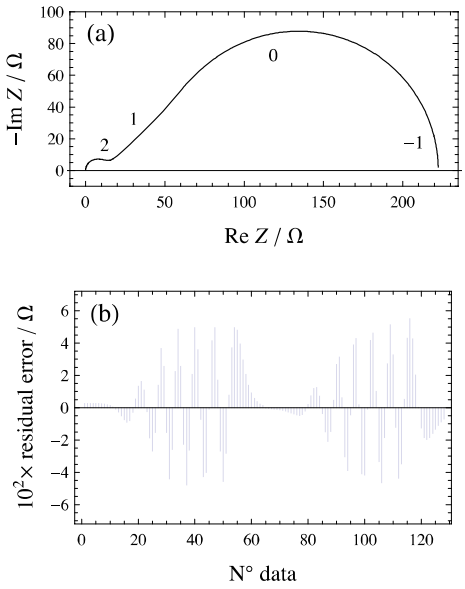

Fig. 5: (a) Nyquist plot for the impedance data (dots) calculated from Eqs. (4) and (21), and best-fitting impedance graph (solid line) obtained from a Voigt circuit with 6 RC elements. Parametrization of the impedance graph with $\log\left(f/\mathrm{Hz}\right)$. (b) Residual errors (dots) of the complex nonlinear least squares fit for the real parts (data N° 1 to 64) and the imaginary parts (data N° 65 to 128) of the electrode impedance at increasing frequencies from left to right. Parameter values: $R_\mathrm{t} = 12.5\ \Omega$, $R_\mathrm{d} = 210\ \Omega$, $\delta = 1.8\times10^{-3}\mathrm{cm}$, $D = 6.5\times10^{-6}\mathrm{cm^2s^{-1}}$, and $C_\mathrm{dl} = 4.0\times10^{-6}\mathrm{F}$.

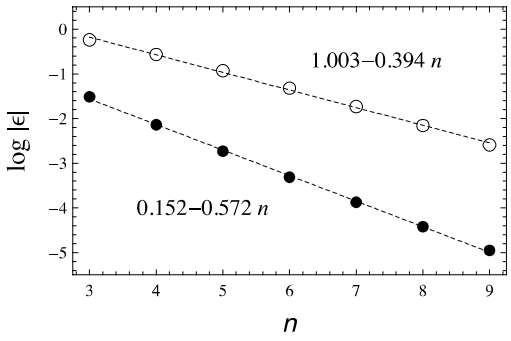

Fig. 6: Decimal logarithm of the absolute value of relative deviation of the best-fit estimates $\hat{\tau}_1$ (filled circles) and $\hat{\tau}_2$ (open circles) from the time constants τ_1 and τ_2, respectively, plotted as a function of the number of RC elements used in the Voigt circuit. Best linear fits (dashed lines). Same parameter values as in Fig. 5.

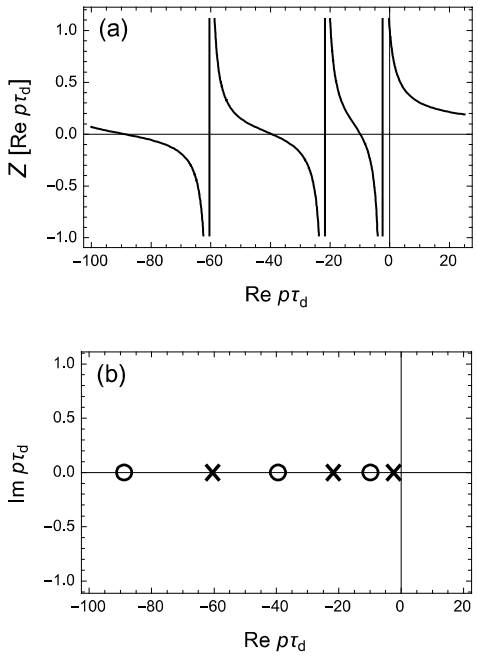

Fig. A.1: (a) Real-p impedance and (b) the first three poles (crosses) and three zeros (circles) of the normalized electrode impedance, $Z(p)/R_\mathrm{d} = \left\{ p\tau_\mathrm{d} r_\tau + (p\tau_\mathrm{d})^{1/2} \coth\left[(p\tau_\mathrm{d})^{1/2} \right] \right\}^{-1}$, calculated from Eqs. (4) and (12) at $r_\tau = 0.01$.